Supporting Information

Dirhodium Complexes as Electrocatalysts for CO_2 Reduction to HCOOH: Role of Steric Hindrance on Selectivity

Hemanthi D. Manamperi, Curtis E. Moore, and Claudia Turro*

Department of Chemistry and Biochemistry, The Ohio State University, Columbus, OH 43210, USA
Corresponding author: turro.1@osu.edu

Synthesis and Characterization

Materials. All materials were used as received without further purification unless otherwise noted. $Rh_2(OAc)_4$ was obtained from Pressure Chemicals. Formic acid (≥95.0%), triethyloxonium tetra fluoroborate (1.0 M in methylene chloride), 1,10-phenanthroline (99%), electrochemical grade tetrabutyl ammonium hexafluorophosphate (≥99.0%) and 4′-methylacetanilide (NtolylacamH) were purchased from Sigma-Aldrich. *Cis*-$Rh_2(acam)_2(phen)_2Cl_2$ was prepared by following previously published methods.[S1] p-toluidine was recrystallized from petroleum ether prior to use. It should be noted that our attempts to synthesize *cis*-H,T-$[Rh_2(L)_2(phen)_2]^{2+}$, where L = acetamidate, resulted in a mixture of the (H,H) and (H,T) isomers and we were unsuccessful in their isomer separation. Therefore, for complex **1**, trifluoroacetamidate was employed as the bridging ligand instead of acetamidate, with a trifluoro methyl substituent at the central carbon of the bridgehead as opposed to methyl group at the same position in complexes **2** and **3**. The presence of electron withdrawing CF_3 group in trifluoro acetamidate bridging ligand allowed us to follow a different synthetic route that exclusively resulted in the formation of the (H,T) isomer.

$[Rh_2(acam)_2(phen)_2][BF_4]_2$ (1). $Rh_2(acam)_2phen)_2Cl_2$ (100 mg, 0.1 mmol) was stirred in CH_3CN in the presence of 3 equivalents of $NaBF_4$ at room temperature. After 24 hours solution was filtered through celite and reduced in volume. Product was isolated as a yellow/orange colored solid upon adding excess diethyl ether (70 mg, 63 % yield). ^{1}H NMR in CD_3CN, (400 MHz): δ 8.55 (d, J = 4.8 Hz, 2H), 8.29 (t, J = 6.0 Hz), 8.06 (d, J = 7.2 Hz, 1H), 7.77 (m, 1H), 7.68 (d, J = 8.8 Hz, 1H), 7.59 (d, J = 8.8 Hz, 1H), 7.32 (t, J = 6.0 Hz, 1H). ESI-MS: $[\mathbf{1}]^{2+}$ = 394.99.

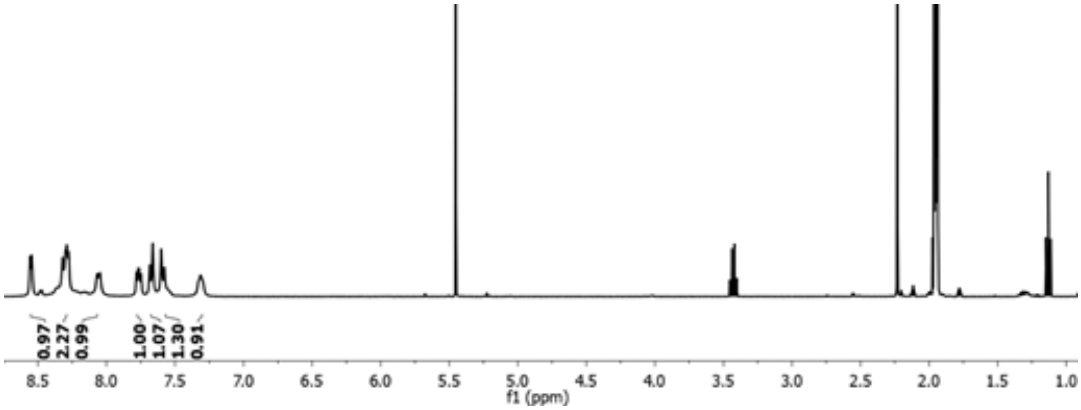

Figure S1. ^{1}H NMR of **1** in CD_3CN at 400 MHz.

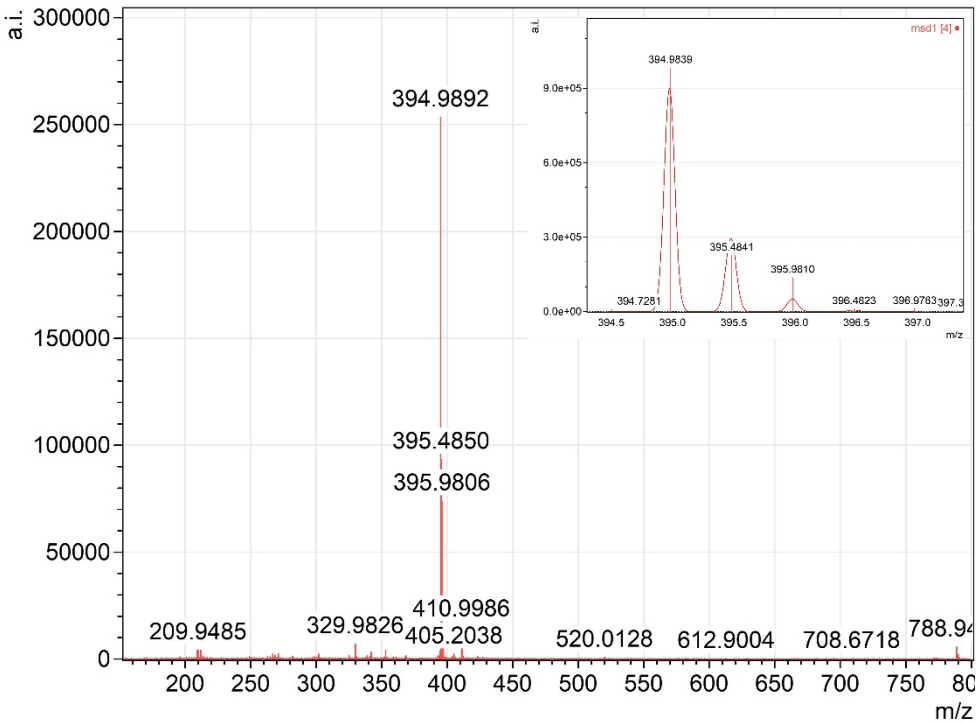

Figure S2. ESI-MS spectrum of **1**.

$[Rh_2(Ntolylacam)_2(phen)_2][BF_4]_2$ (2). $Rh_2(OAc)_4$ (200 mg, 0.45 mmol) and 20 equivalents of N-tolylacetamide were heated at reflux under N_2 for 72 hour in 10 ml of anhydrous chlorobenzene. Then the solvent was removed by rotary evaporation and residue was dissolved in ~100 ml of diethyl ether. Upon slow evaporation of solvent crystallization of the excess N-tolylacetamide ligand was noticed. At this point the solution was decanted into a separate beaker and this process was continued until no more ligand precipitation was noticed. Rh_2(N-tloylacam)$_4$ was obtained as a dark green colored powder. ESI-MS: $[Rh_2(Ntolylacam)_4]^+$ = 798.20. This was used without further purification for the next step. Next 30 mL of CH_3CN was added to Rh_2(N-tolylacam)$_4$ followed by 1 ml of triethyloxonium tetrafluoroborate (1 M in CH_2Cl_2), to result in an immediate color change from blue/purple to pink/magenta. This solution was stirred at 40 ^oC for 4 hours and then the stirring was continued for additional 12 hours at room temperature. The solution was then filtered through celite, reduced in volume and was added excess diethyl ether to precipitate $[Rh_2(Ntolacam)_2(CH_3CN)_6][BF_4]_2$ as a magenta colored solid. This solid was washed twice with diethyl ether and dried in air. ESI-MS: $[Rh_2(Notolacam)_2(CH_3CN)_n]^{2+}$ 312.55 (n = 3), 292.04 (n = 2), 271.52 (n = 1) and 251.00 (n = 0). The highly hydroscopic nature of the product prevented its analysis using ^1H NMR. Next $[Rh_2(N\text{-}tolacam)_2(CH_3CN)_6][BF_4]_2$ was combined with 2.2 equivalents of 1,10-phenanthroline in 30 mL CH_3CN and the solution was gently refluxed under N_2 for 16 hours. Upon completion of the reaction, the solvent was reduced in volume and the product was precipitated by adding excess diethyl ether as an olive green colored powder. Next the crude product was extracted into dichloromethane and the insoluble solid product, which mainly consist of $Rh(phen)_3(BF_4)_3$ was discarded. (151 mg, 32% overall yield). X-ray quality crystals were obtained by slow diffusion of diethyl ether into a concentrated solution of **2** in CH_3CN with added pyridine (0.2% v/v pyridine in CH_3CN) ^1H NMR in CD_3CN, (400 MHz): δ 9.20 (d, J = 4.8 Hz, 1H, phen), 8.34 (d, J = 7.6 Hz, 1H, phen), 8.22 (d, J = 5.2 Hz, 1H, phen), 8.00-7.97 (m, 2H, phen), 7.67 (d, J = 8.8 Hz, 1H, phen), 7.58 (d, J = 8.8 Hz, 1H, phen), 7.28-7.21 (m, 5H, phen+4'-methylacetanilide), 2.42 (s, 3H, CH_3), 2.36 (s, 3H, CH_3). ESI-MS: $[\mathbf{2}]^{2+}$ m/z = 431.10.

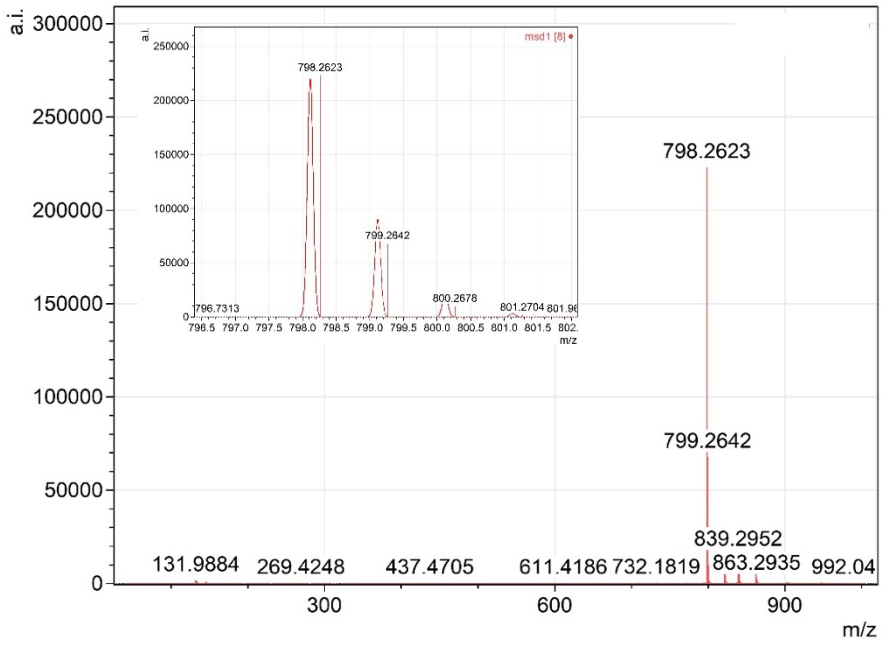

Figure S3. ESI-MS spectrum of Rh_2(Ntolacam)$_4$.

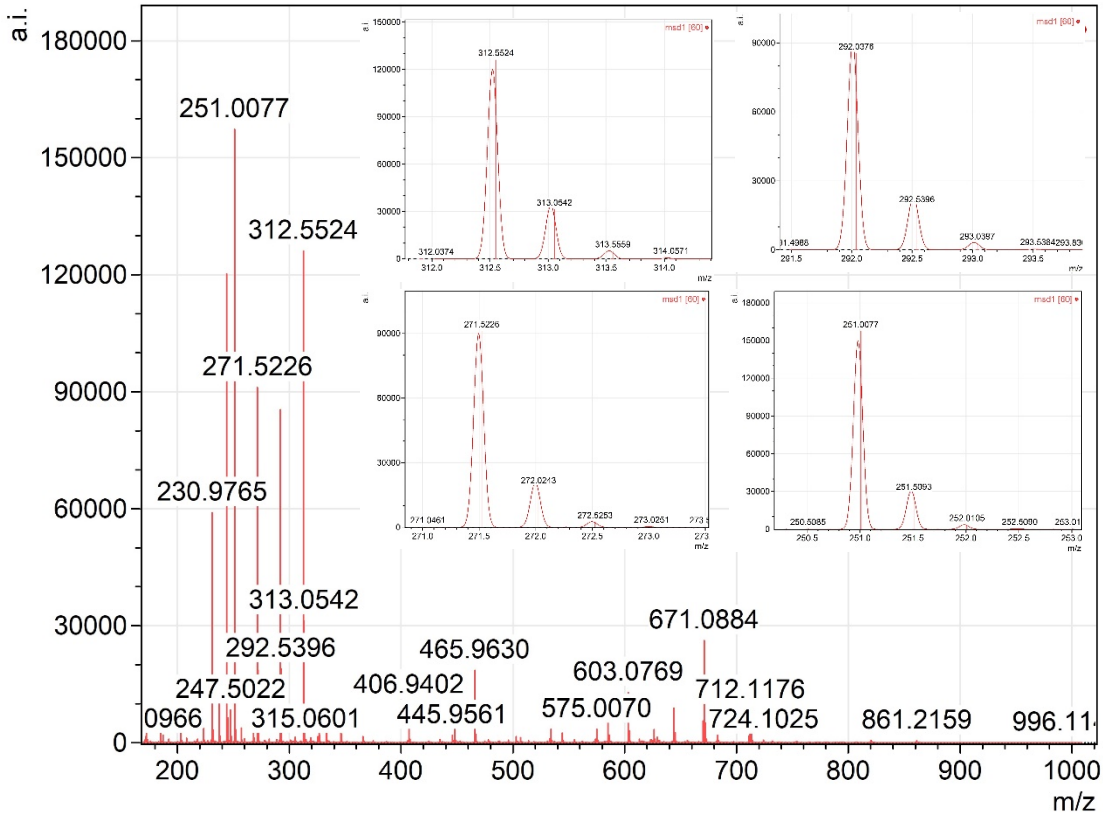

Figure S4. ESI-MS spectrum of [Rh_2(Ntolacam)$_2$(CH_3CN)$_6$](BF_4)$_2$.

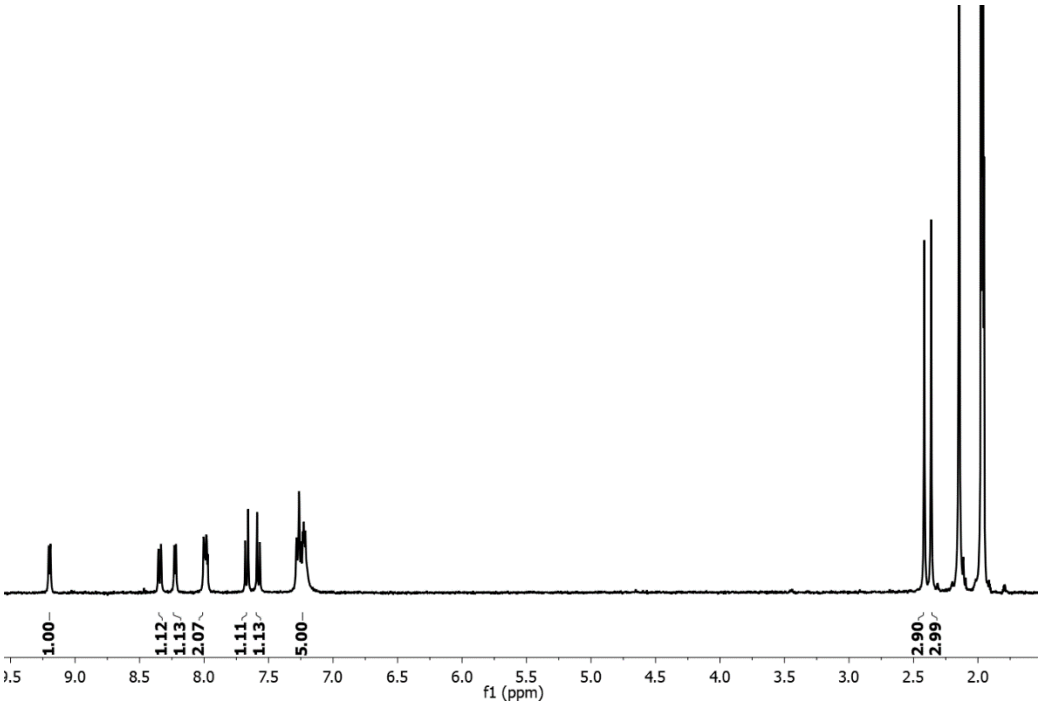

Figure S5. ^{1}H NMR of **2** in CD_3CN at 400 MHz.

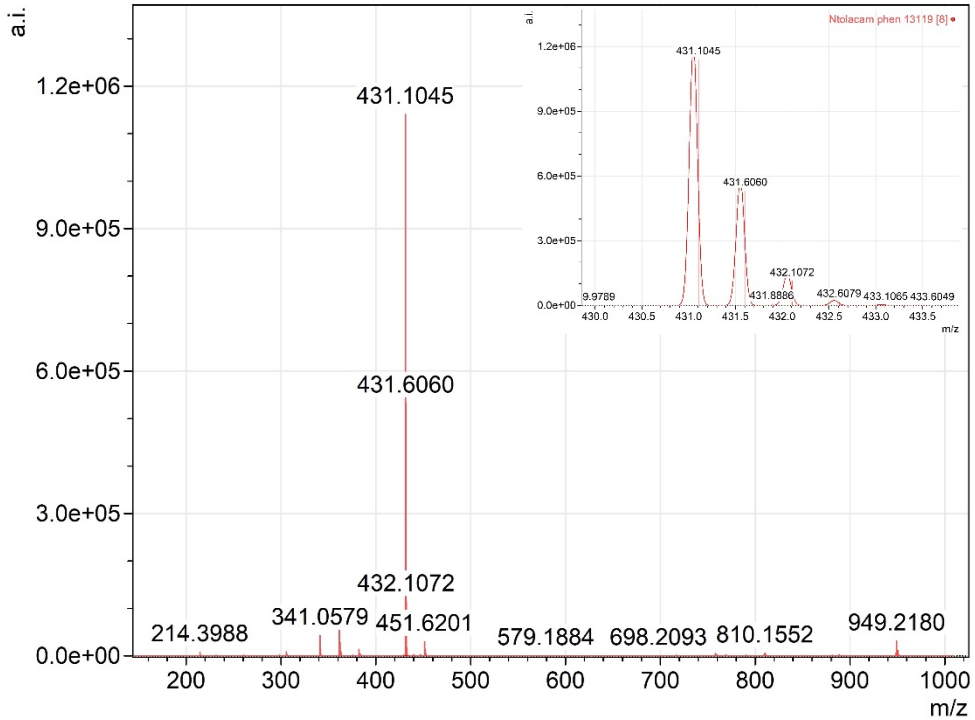

Figure S6. ESI-MS spectrum of **2**.

N,N′-bis(tolyl)ethanimidamidine (MeDTolFH). This ligand precursor was synthesized by following similar synthesis method reported for N,N′ -diarylethanimidine,[S2] by substituting p-toluidine for aniline. Yield (72%). ^{1}H NMR in $CDCl_3$, (400 MHz): δ 7.14-7.04 (m, 8H), 2.33 (s, 6H), 2.00 (s, 3H).

Rh_2(MeDTolF)$_4$. This complex was synthesized using a molten reaction as reported elsewhere for similar paddle wheel formamidinate complexes.[S3] ^{1}H NMR in $CDCl_3$, (400 MHz): δ 6.87 (d, J = 7.6 Hz, 4H), 6.05 (d, J = 7.6 Hz, 4H), 2.27 (s, 6H), 1.74 (s, 3H), ESI-MS: $[Rh_2(MeDTolF)_4]^+$ = 1154.36.

$[Rh_2(MeDTolF)_2(phen)_2][BF_4]_2$ (**3**). This complex was synthesized by following a similar route as for **2**, starting with $Rh_2(MeDToLF)_4$. Yield: 41%. ^{1}H NMR in CD_3CN, (400 MHz): δ 8.64 (br s, 2H), 8.17 (d, 2H, J = 4.0 Hz), 7.63 (s, 4H), 7.10 (d, 2H, J = 6.8 Hz), 6.96 (s, 4H), 2.29 (s, 6H) and 2.19 (s, 3H), ESI-MS: $[Rh_2(MeDTolF)_2(phen)_2]^{2+}$ = 520.12 and $[Rh_2(MeDTolF)_2(phen)_2)(BF_4)]^+$ = 1127.21.

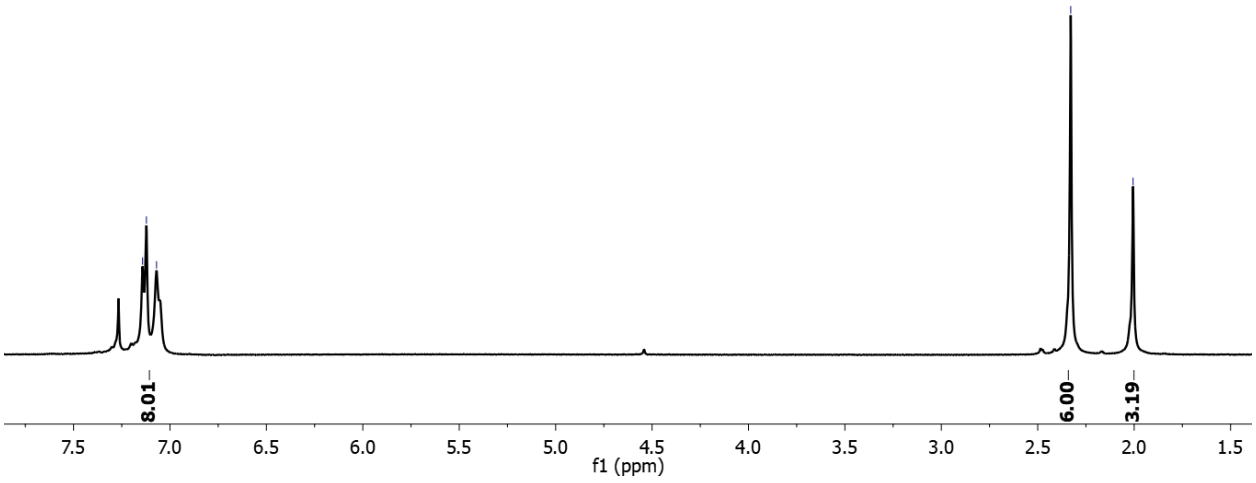

Figure S7. ^{1}H NMR of MeDTolFH in CD_3Cl at 400 MHz.

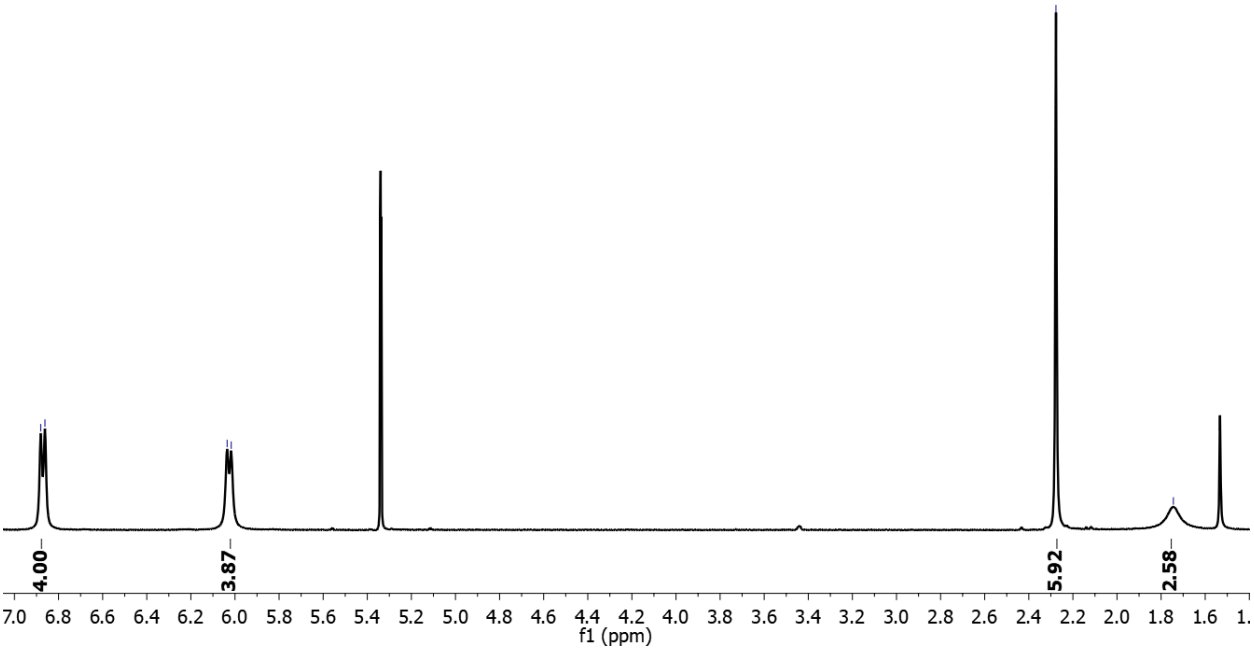

Figure S8. ^{1}H NMR of $Rh_2(MeDTolF)_4$ in CD_2Cl_2 at 400 MHz.

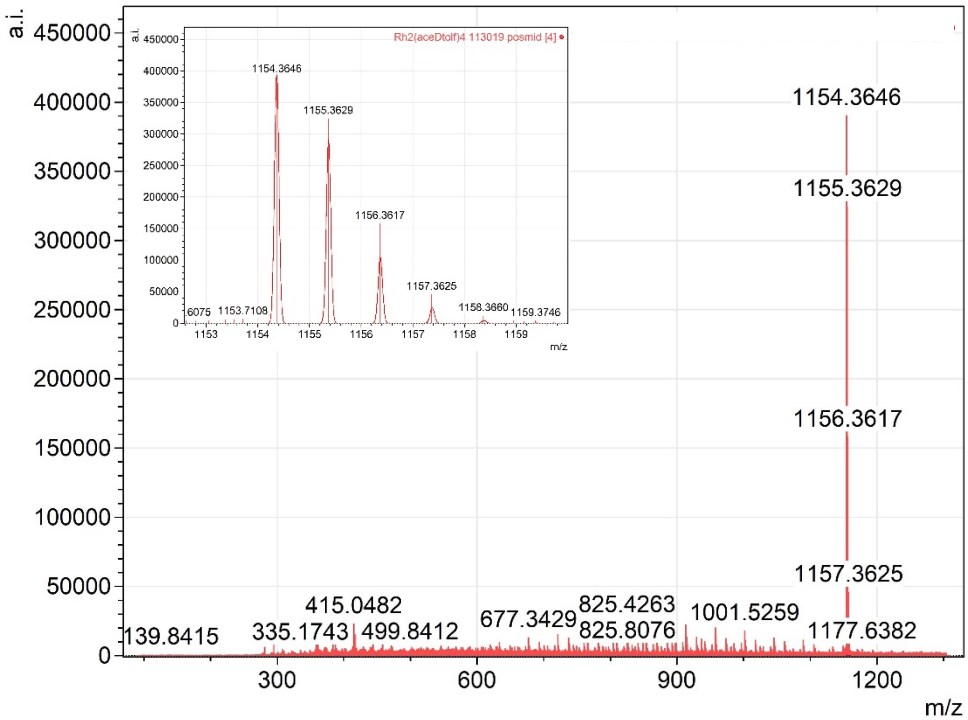

Figure S9. ESI-MS spectrum of $Rh_2(MeDTolF)_4$.

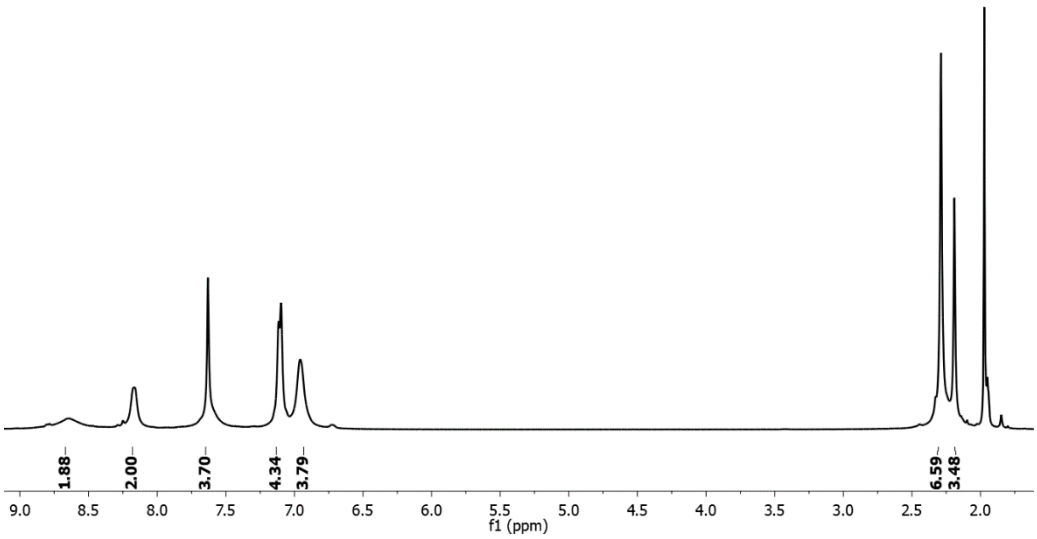

Figure S10. ^{1}H NMR of **3** in CD_3CN at 400 MHz.

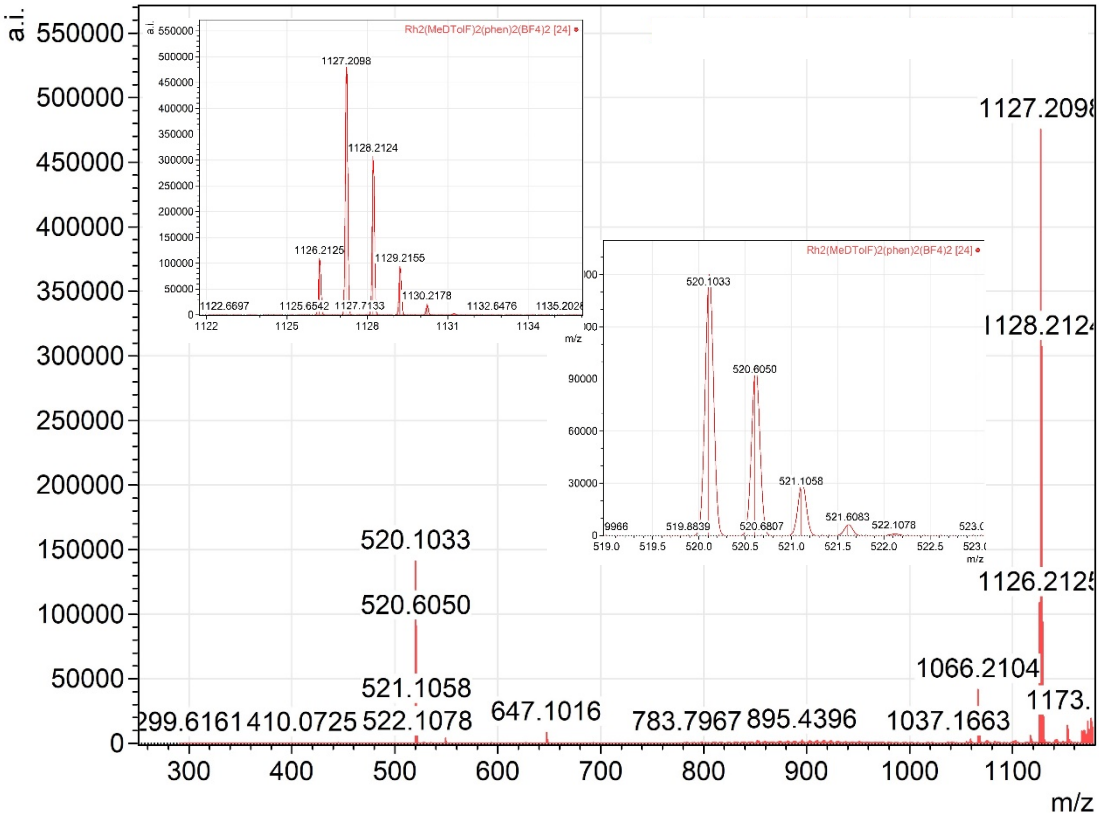

Figure S11. ESI-MS spectrum of **3**.

X-ray crystal structure

The molecular structure of **2-py$_2$** was determined by X-ray crystallography and consistent with two rhodium centers bridged by two N-tolylacetamide ligands in *cis*-H,T geometry (Figure S12a). The remaining equatorial sites and the two axial sites are occupied by two chelating phen (1,10-phenanthroline) ligands and pyridine molecules respectively. The Rh−Rh bond distance was 2.5785(4) Å, which is ~0.03 Å shorter than the bond distance reported for **1-py$_2$** (2.612 Å) with similar pyridine coordination at both axial sites.[S1] This may arise from the differences in electronic and steric properties between trifluoroacetate and N-tolylacetamidate bridging ligands, with former being more electron withdrawing and with no bulky groups at the vicinity of axial sites provided by the bridging ligand, and thus resulting in a longer Rh−Rh bond. Complex **3** possesses a Rh−Rh distance of 2.5329(5) and attributes to the shortest Rh−Rh distance within the series. It is also interesting to note that, between complexes **1** − **3**, complex **3** has an acetonitrile molecule coordinated at one axial site, whereas, complexes **1** and **2** has two pyridine molecules coordinated at both axial sites (Figure S12b).

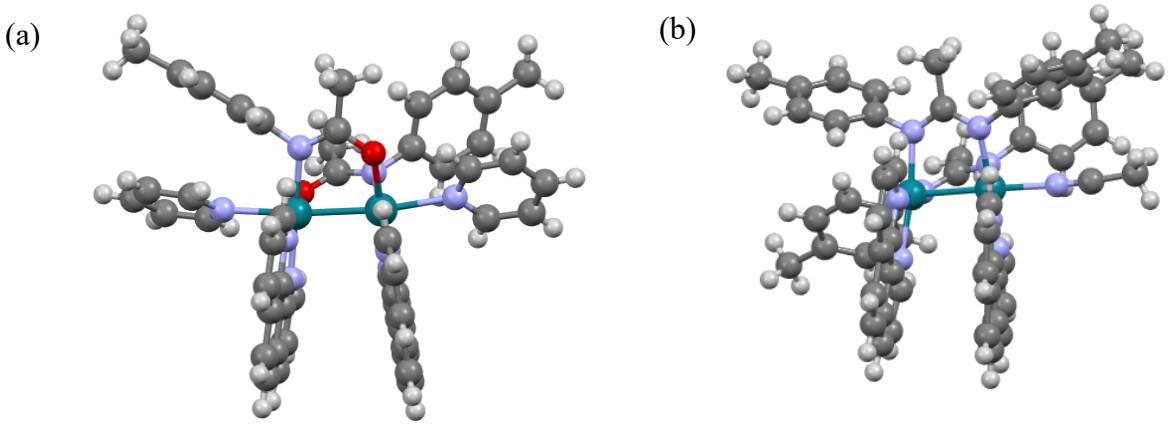

Figure S12. Crystal structures of (a) **2-py$_2$** and (b) **3** (ellipsoid plots are drawn at 50% probability).

Table S1. Crystal data and structure refinement for **2-py$_2$** and **3**.

	2-py$_2$	**3**
Empirical formula	$C_{52}H_{46}B_2F_8N_8O_2Rh_2$	$C_{62}H_{63}B_2F_8N_9ORh_2$
Molecular formula	$C_{42}H_{36}N_6O_2Rh_2$, 2(BF_4), 2(C_5H_5N)	$C_{56}H_{50}N_8Rh_2$, 2(BF_4), C_2H_3N, $C_4H_{10}O$
Formula weight	1194.41	1329.65
Temperature	100 K	100.0 K
Wavelength	0.71073 Å	0.71073 Å
Crystal system	Monoclinic	Orthorhombic
Space group	P 1 21/n 1	Pbca
Unit cell dimensions	a = 11.9710(7) α= 90° b = 34.5822(18) Å β= 97.196(2)° c = 12.0112(6) Å γ = 90°	a = 22.1265(5) Å α= 90° b = 20.9437(5) Å β= 90° c = 24.5322(6) Å γ = 90°
Volume	4933.3(5) Å^3	11368.5(5) Å^3
Z	4	8
Density (calculated)	1.608 Mg/m^3	1.554 Mg/m^3
Absorption coefficient	0.750 mm^{-1}	0.659 mm^{-1}
F(000)	2408	5424
Crystal size	0.164 x 0.127 x 0.059 mm^3	0.158 x 0.121 x 0.097 mm^3
Crystal color, habit	Dark Red Block	Dark Red Block
Theta range for data collection	2.826 to 26.378°	1.575 to 24.998°
Index ranges	-14<=h<=14, -43<=k<=43, -15<=l<=15	-26<=h<=26, -24<=k<=24, -29<=l<=29
Reflections collected	50853	161251
Independent reflections	10076 [R(int) = 0.0528, R(sigma) = 0.0447]	10012 [R(int) = 0.1088, R(sigma) = 0.0471]
Absorption correction	Semi-empirical from equivalents	Semi-empirical from equivalents
Max. and min. transmission	0.0932 and 0.0667	0.0916 and 0.0617
Refinement method	Full-matrix least-squares on F^2	Full-matrix least-squares on F^2
Data / restraints / parameters	10076 / 60 / 708	10012 / 0 / 766
Goodness-of-fit on F^2	1.082	1.060
Final R indices [I>2sigma(I)]	R1 = 0.0421, wR2 = 0.0756	R1 = 0.0472, wR2 = 0.0994
R indices (all data)	R1 = 0.0577, wR2 = 0.0801	R1 = 0.0800, wR2 = 0.1145
Extinction coefficient	n/a	n/a
Largest diff. peak and hole	0.588 and -1.110 e.Å^{-3}	1.037 and -0.668 e.Å^{-3}

Methods and Instrumentation. Electrochemical experiments were carried out on a BASi model CV-50W voltammetric analyzer (Bioanalytical Systems, Inc.; West Lafayette, IN, USA). Cyclic voltammetry (CV) experiments were carried out with 0.5 mM Rh_2 solutions with a glassy carbon disk working electrode (3 mm diameter), platinum wire auxiliary electrode, and Ag/AgCl (3 M NaCl) reference electrode (calibrated with ferrocene; $Fc^{0/+}$ = 0.438 vs Ag/AgCl) and the solutions were purged with either N_2 or CO_2 prior to each trial. Bulk electrolysis experiments were conducted in a custom made, air-tight two-compartment cell with a glassy carbon rod working electrode, platinum coil counter electrode, and Ag/AgCl (3 M NaCl) reference electrode. For each trial, a 5 mL solution of 0.5 mM Rh_2 in CH_3CN containing 0.1 M $TBAPF_6$ and 3 M H_2O was used. Both the auxiliary and working compartments were purged with either N_2 or CO_2 for 20 minutes prior to applying a negative bias. After one hour, a 200 μL aliquot of the 35 mL head space was removed using a Hamilton gas-tight syringe and injected into a Shimadzu GC-2014 gas chromatograph (GC) with a TCD-2014 thermal conductivity detector with Ar as the carrier gas, and equipped with a 5 Å molecular sieves packed column (6 ft long x 1/8 in OD x 201 mm ID). H_2 detection by GC was accomplished at an injection temperature of 41 ^oC, a column temperature of 30 ^oC, a detector temperature of 150 ^oC, a detector current of 60 mA and a gas flow of 25 mL/min. The H_2 in each injection was quantified using an external calibration curve. HCOOH was quantified using ^1H NMR with an internal standard as explained elsewhere.[S4] Bulk electrolysis experiments under identical conditions were carried out in the absence of catalyst as control experiments, which did not result in the production of any HCOOH or H_2, showing that HCOOH stems from CO_2 and not from glassy carbon electrode decomposition.

Spectroelectrochemistry experiments were carried out using a custom-made air-tight quartz cell with a 1 cm path length as the working compartment that was separated from the auxiliary compartment by a glass frit. A glassy carbon rod, a Ag/AgCl reference electrode and a Pt coil were used as working, reference, and counter electrodes, respectively. The spectral changes were monitored upon applying a sufficiently negative potential to accumulate the desired reduced species.

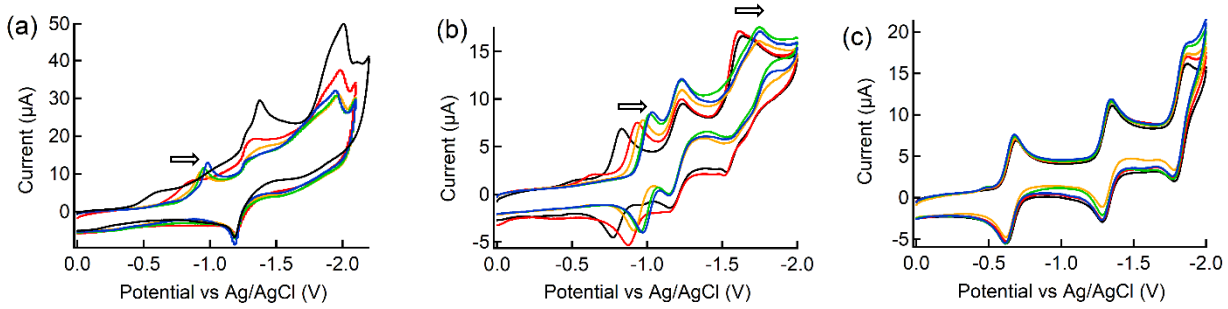

Figure S13. CVs of (a) **1**, (b) **2** and (c) **3** collected in the presence of 0 mM (black), 5 (red), 10 (orange), 43 (green) and 68 (blue) mM pyridine, collected in CH_3CN / 0.1 M $TBAPF_6$ at 0.1 V/s scan rate under N_2.

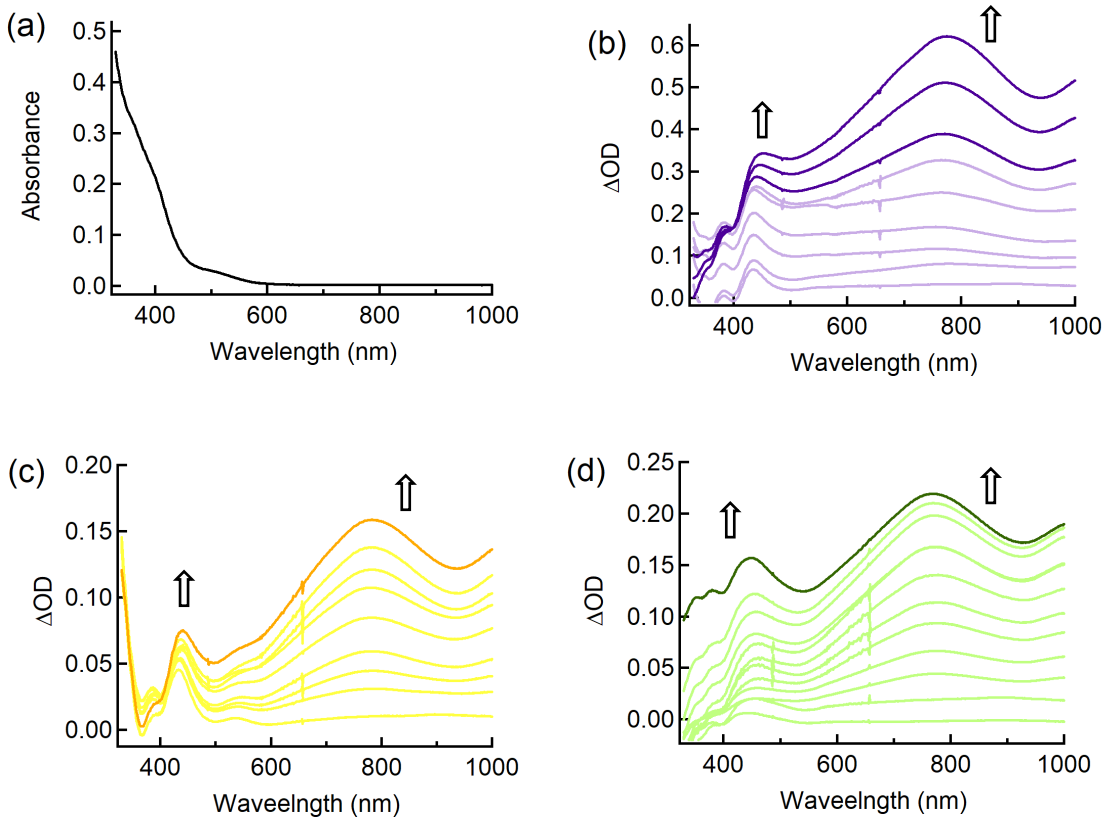

Figure S14. (a) Electronic absorption spectrum of **1** in CH_3CN and difference spectra for the electrolysis of **1** at −1.60 V in CH_3CN / 3 M H_2O under (b) CO_2, (d) N_2 and (c) in the absence of H_2O under N_2 at −1.0 V (*vs* Ag/AgCl).

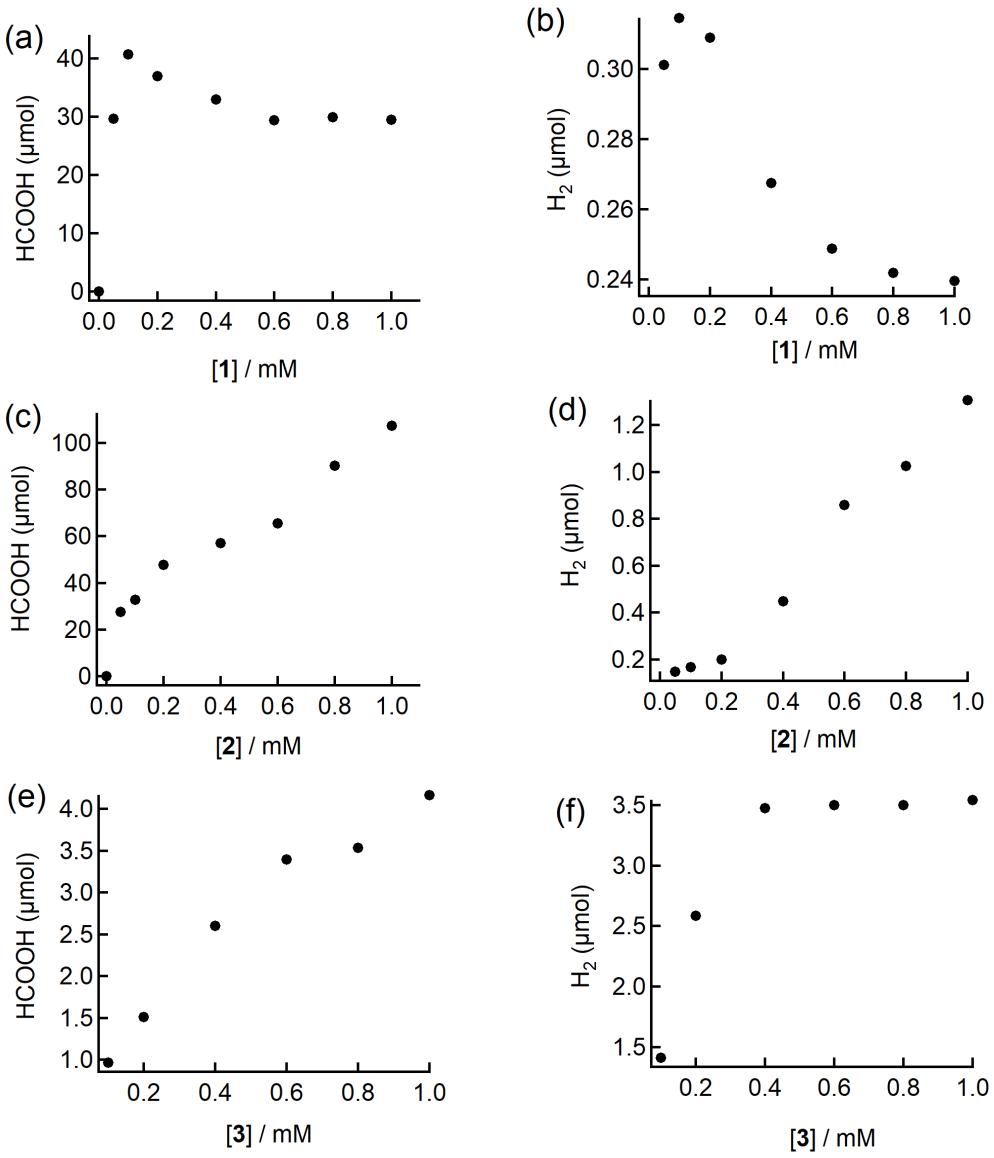

Figure S15. Variations of the formation of (a), (c), and (e) HCOOH and (b), (d), and (f) H_2 with increasing [Rh_2] concentration, upon electrolyzing a 3 mL solution of Rh_2 in 3 M H_2O / CH_3CN / CO_2 at –1.6 V *vs* Ag/AgCl for 25 minutes with complex (a) and (b) **1**, (c) and (d) **2**, and (e) and (f) and **3**.

H/D Kinetic Isotope Effect

The H/D kinetic isotope effect (KIE) can be broadly defined as the ratio between the rate constants of reactions involving hydrogen to that of deuterium. This concept can be implemented in the CO_2 reduction catalysis by comparing the rates of the reactions employing either H_2O or D_2O as the proton source to aid elucidation of the mechanism. The overall rate of CO_2 reduction, k_{obs} (observed rate constant) with H_2O and D_2O can be compared to determine the H/D KIE.[S5] The value of k_{obs} can be related to the current ratio, i_{cat}/i_p (i_{cat} = catalytic current in the saturated kinetic region, where the current is not limited by the substrate diffusion to the electrode surface and i_p = current in the absence of CO_2 and H_2O/D_2O) according to (1).[S6]

$$\frac{i_{cat}}{i_p} = 2.424\frac{n_{cat}}{n_p}\sqrt{\frac{RTk_{obs}}{n_pFv}} \qquad (1)$$

where n_{cat} is the number of electrons involved in the catalytic process (2 e^-), n_p is the number of electrons for the non-catalytic redox process (1 e^-), R is the ideal gas constant (8.314 V C K^{-1} mol^{-1}), T is temperature (298 K), F is Faraday's constant (96 485 C mol^{-1}), ν is the scan rate (0.1 V s^{-1}). Further, i_{cat} can be determined by the current in the $[H_2O]/[D_2O]$ independent region, and the ratio $(i_{cat}/i_p)^2(H_2O)/(i_{cat}/i_p)^2(D_2O)$ provides the numerical value of H/D KIE.[S7]

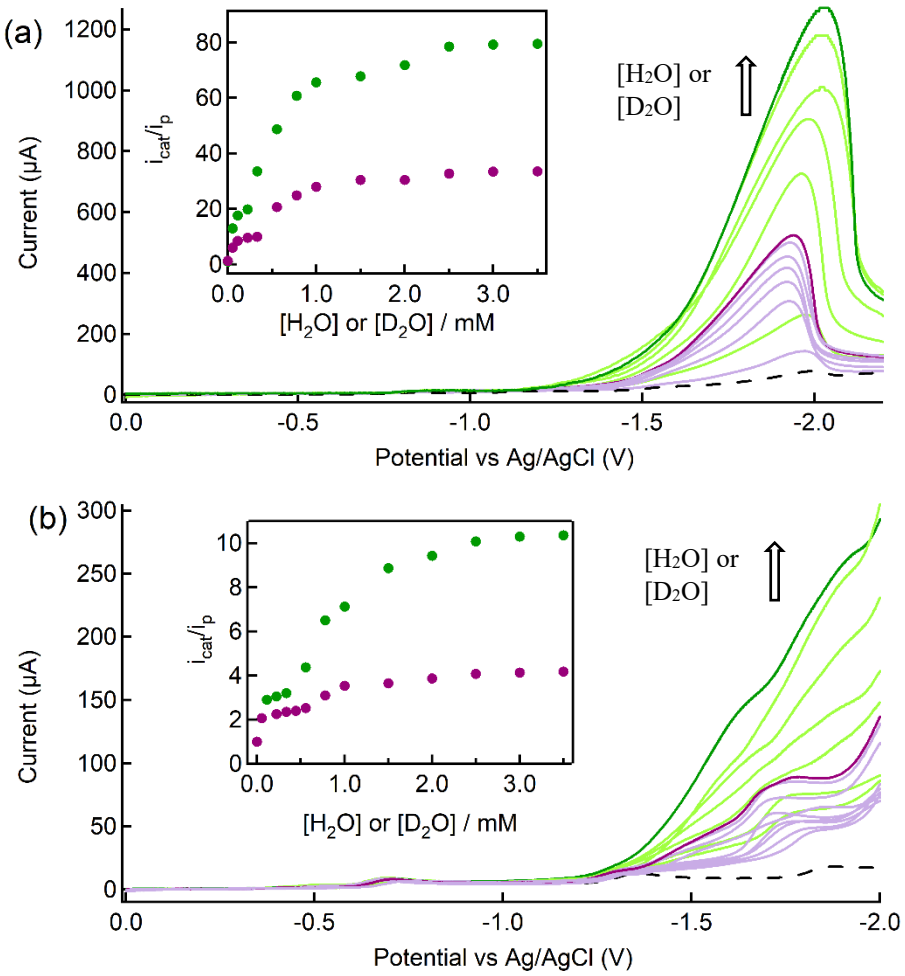

Figure S16. Variation of i_{cat}/i_p with increasing concentrations of H_2O (green) or D_2O (purple) for (a) **2** and (b) **3**; for clarity not all the CVs are shown and only the forward scan is included.

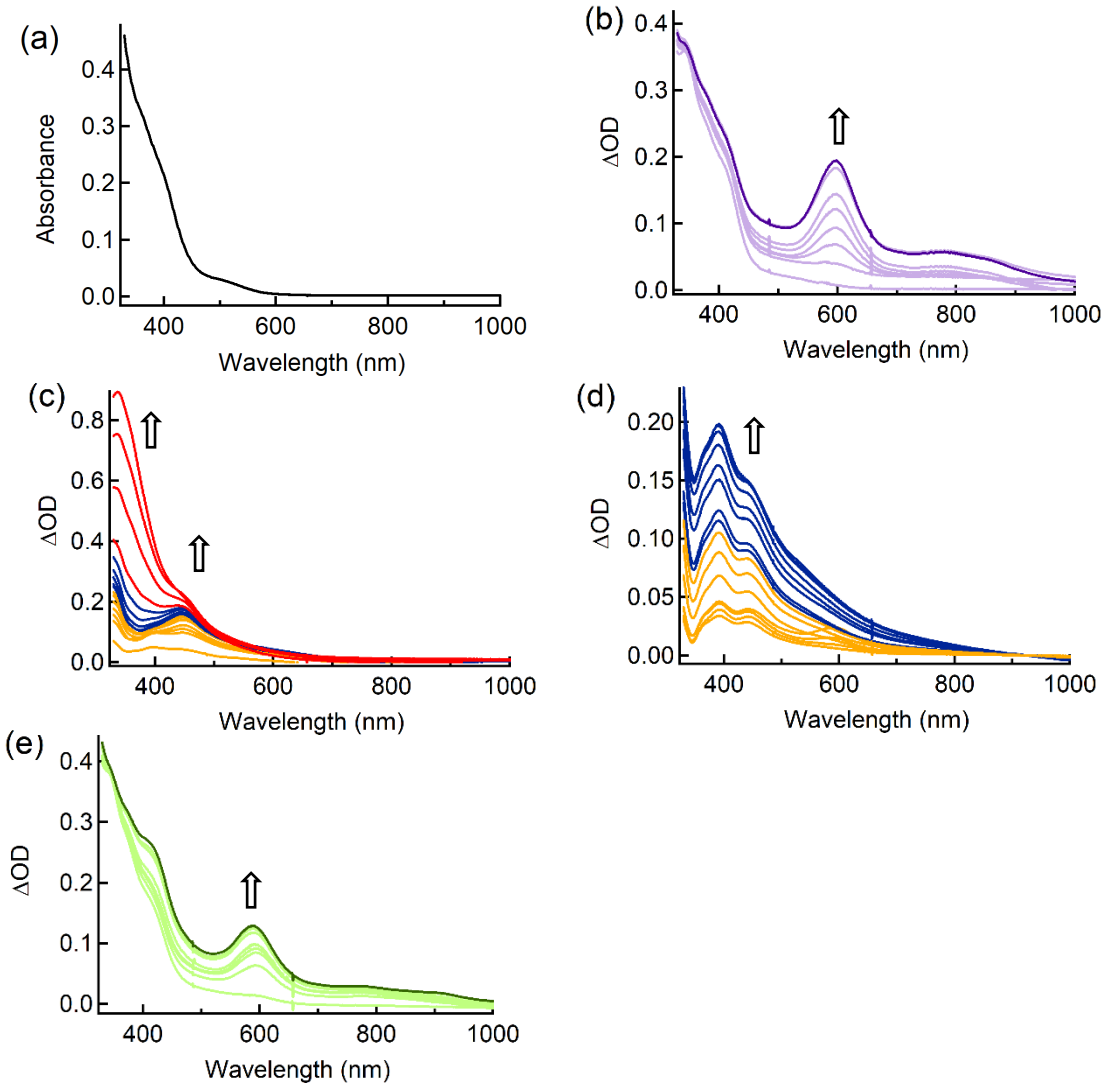

Figure S17. (a) Electronic absorption spectrum of **2** in CH_3CN and difference spectra for electrolysis of **2** at −1.60 V in CH_3CN / 3 M H_2O under (b) CO_2 and (e) N_2 and under N_2 at −1.05 (yellow), −1.45 (blue) and −1.95 V (red) with (c) 0 M and (d) 3 M H_2O. Potentials are *vs* Ag/AgCl.

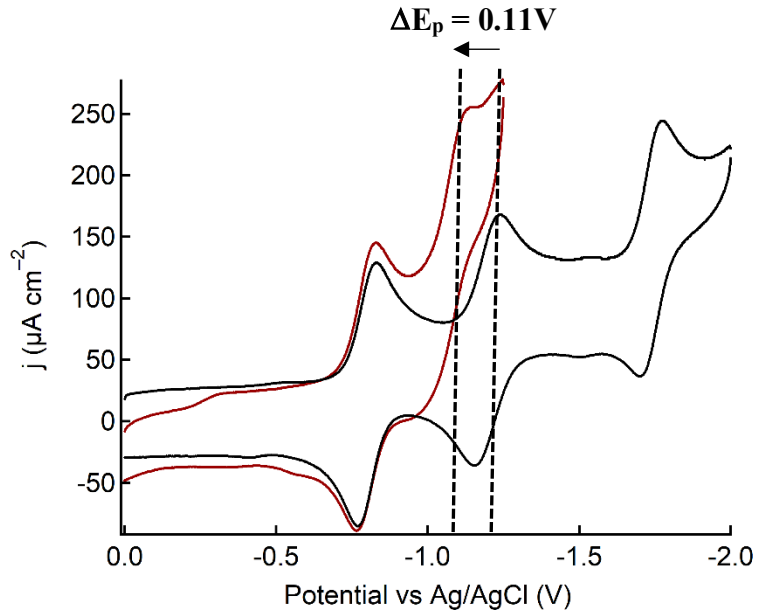

Figure S18. CVs of **2** under N_2 (black) and CO_2 / 3 M H_2O (red) upon reversing the CV scan followed by the 2nd reduction event, collected in CH_3CN / 0.1 M $TBAPF_6$ at 0.1 V/s scan rate.

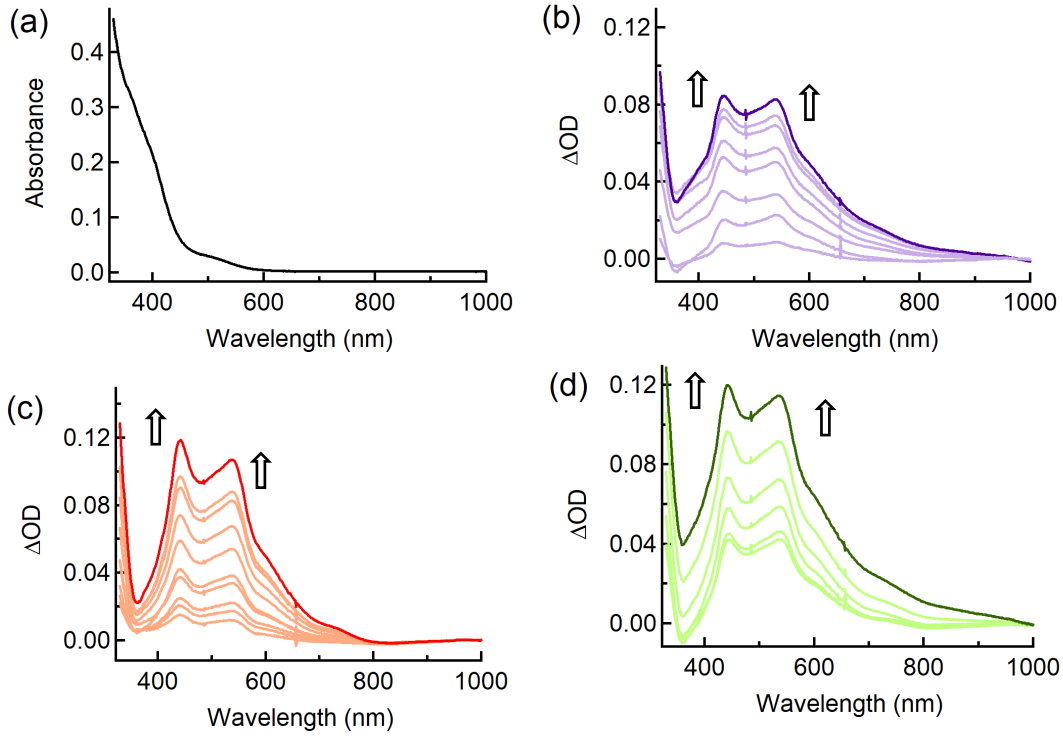

Figure S19. (a) Electronic absorption spectrum of **3** in CH_3CN and difference spectra for electrolysis of **3** at −1.60 V in CH_3CN / 3 M H_2O under (b) CO_2 and (d) N_2 and in the absence of H_2O under N_2 at −1.6 V (*vs* Ag/AgCl).

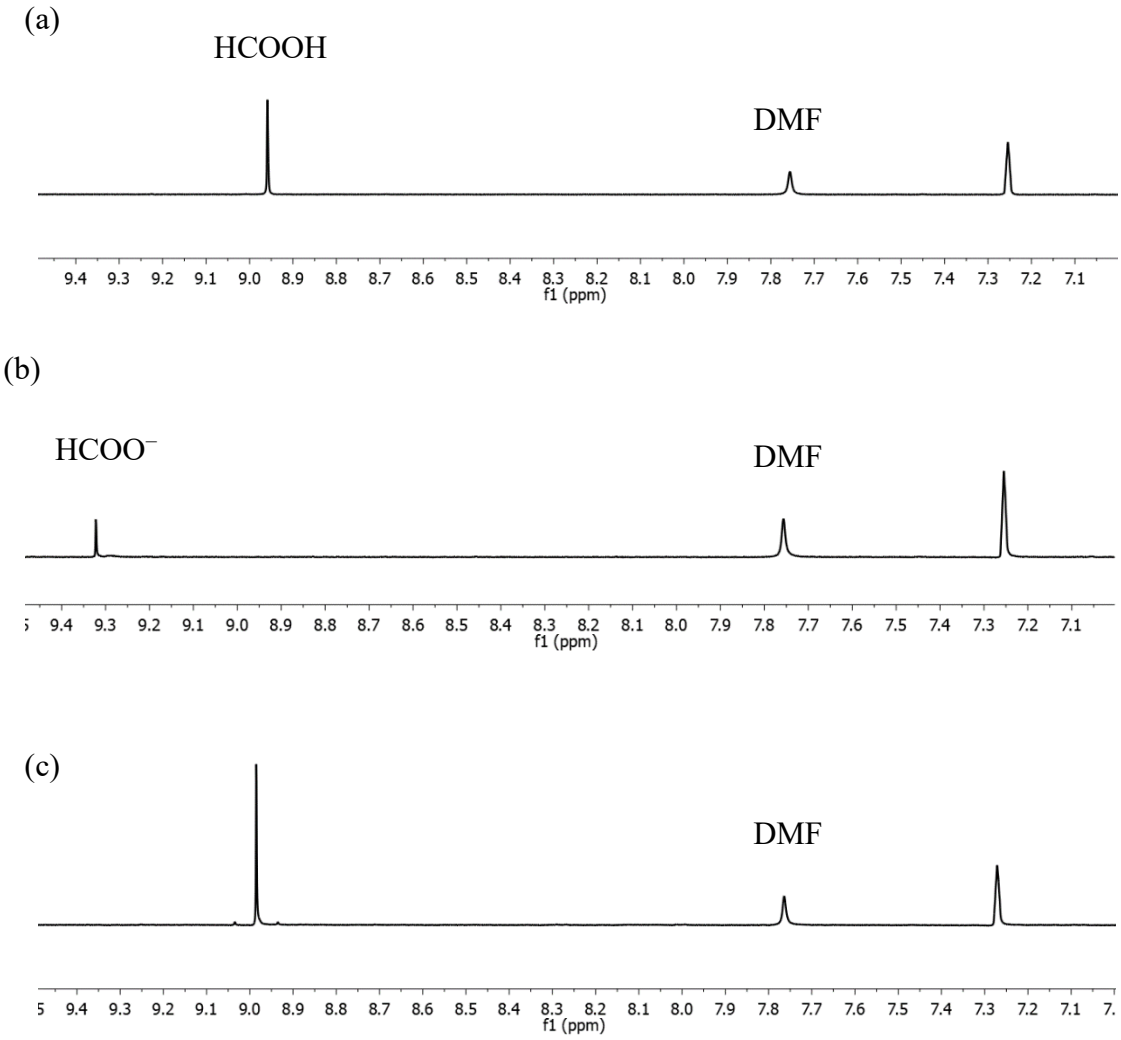

Figure S20. ^{1}H NMR spectra collected with a DMF internal standard in CH_3CN containing 3 M H_2O and 0.1 M $TBAPF_6$ of (a) HCOOH, (b) NaHCOO, and (c) reaction mixture of **2** after one hour electrolysis at –1.6 V *vs* Ag/AgCl under CO_2.

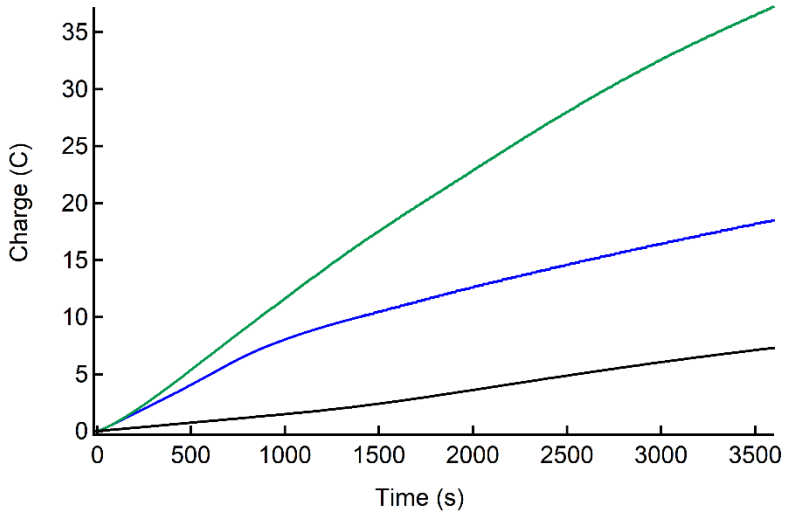

Figure S21. Bulk electrolysis curves for **1** (blue), **2** (green) and **3** (black) for one hour electrolysis with 0.5 mM [Rh_2] at –1.6 V *vs* Ag/AgCl under CO_2.

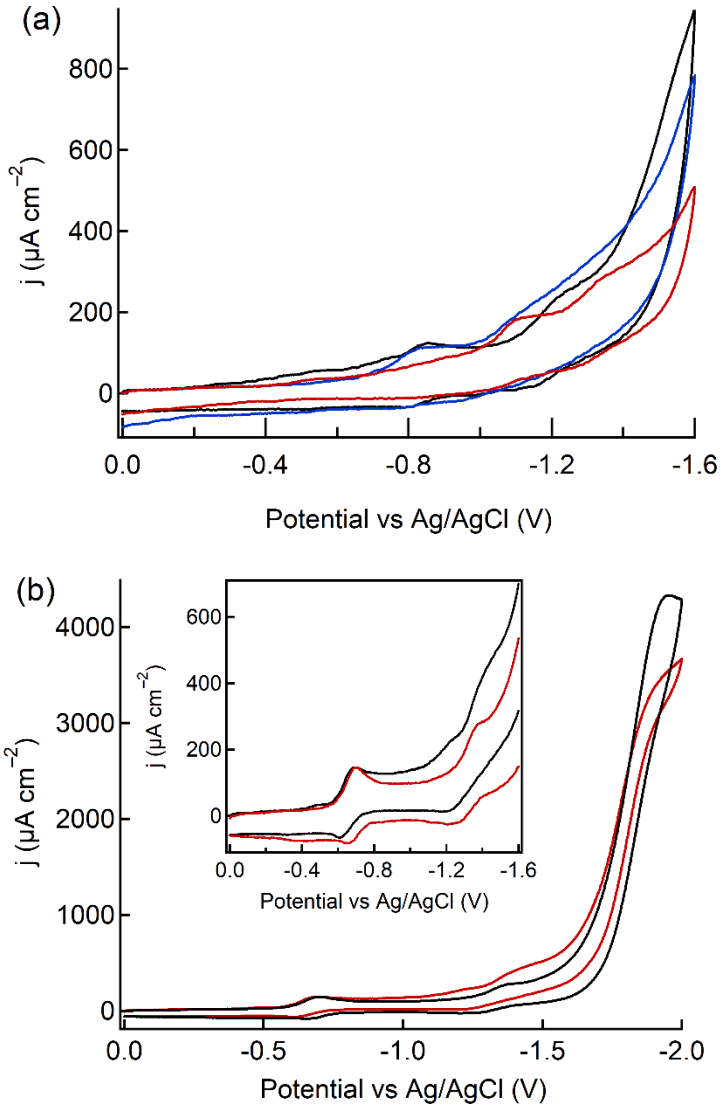

Figure S22. CVs of (a) **2** and (b) **3** collected in 3 M H_2O/CH_3CN under N_2 before (black) and after 1 hour bulk electrolysis with 0.5 mM [Rh_2] at –1.6 V *vs* Ag/AgCl under CO_2 (red). (a) Following the electrolysis at –1.6 V, complex **2** was re-oxidized by applying a positive bias of +0.6 V and then a CV was collected under N_2 (blue trace).

References

S1. M. A. M. Daniels, N. Mehmet and D. A. Tocher, *J. Chem. Soc., Dalton Trans.*, 1991, 2601-2606.
S2. A. M. Fonseca, S. Gonçalves, P. Parpot and I. C. Neves, *Phys. Chem. Chem. Phys.*, 2009, **11**, 6308-6314.
S3. T. Ren, C. Lin, E. J. Valente and J. D. Zubkowski, *Inorg.Chim. Acta*, 2000, **297**, 283-290.
S4. H. D. Manamperi, S. E. Witt and C. Turro, *ACS Appl. Energy Mater.*, 2019, **2**, 7306-7314.
S5. A. Taheri, C. R. Carr and L. A. Berben, *ACS Catal.*, 2018, **8**, 5787-5793.
S6. T. A. White, S. E. Witt, Z. Li, K. R. Dunbar and C. Turro, *Inorg. Chem.*, 2015, **54**, 10042-10048.
S7. B. M. Ceballos and J. Y. Yang, *Proc. Natl. Acad. Sci. U.S.A.*, 2018, **115**, 12686.